

Journal of Materials Chemistry A

Accepted Manuscript

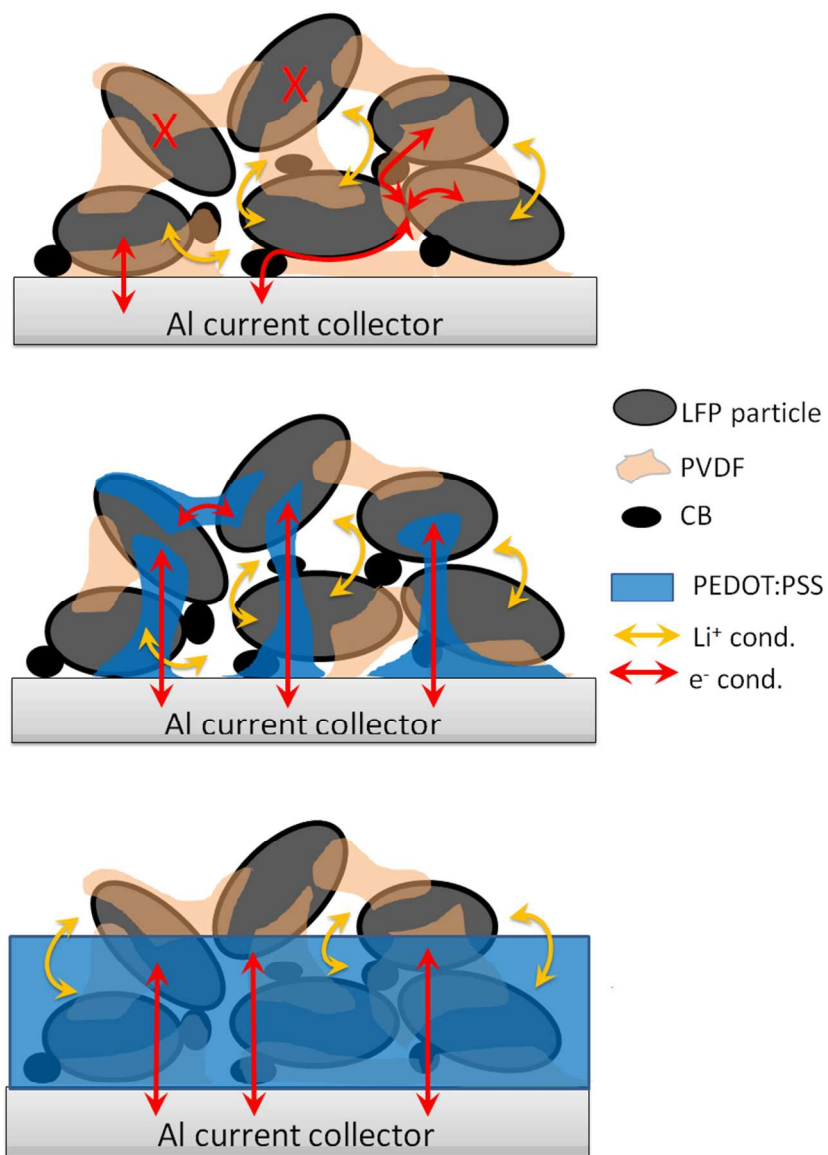


This is an *Accepted Manuscript*, which has been through the Royal Society of Chemistry peer review process and has been accepted for publication.

Accepted Manuscripts are published online shortly after acceptance, before technical editing, formatting and proof reading. Using this free service, authors can make their results available to the community, in citable form, before we publish the edited article. We will replace this *Accepted Manuscript* with the edited and formatted *Advance Article* as soon as it is available.

You can find more information about *Accepted Manuscripts* in the [Information for Authors](#).

Please note that technical editing may introduce minor changes to the text and/or graphics, which may alter content. The journal's standard [Terms & Conditions](#) and the [Ethical guidelines](#) still apply. In no event shall the Royal Society of Chemistry be held responsible for any errors or omissions in this *Accepted Manuscript* or any consequences arising from the use of any information it contains.



Designing of lithium iron phosphate by poly(3,4 ethylenedioxythiophene) for high performance battery

227x327mm (96 x 96 DPI)



Judicious design of lithium iron phosphate electrodes by poly(3,4-ethylenedioxythiophene) for high performance battery

Daniel Cíntora-Juárez,^a Carlos Pérez-Vicente,^a Samrana Kazim,^b Shahzada Ahmad^{b*} and José Luis Tirado^a

Received 00th January 20xx,
Accepted 00th January 20xx

DOI: 10.1039/x0xx00000x

www.rsc.org/

Abstract: LiFePO₄ electrodes were built in different architectures using poly(3,4-ethylenedioxythiophene)-polystyrene sulfonate (PEDOT:PSS) mixed conductor as an additive. Conductivity enhancement of PEDOT:PSS was achieved by addition of ethylene glycol and dimethyl sulfoxide solvent. The amount of conducting polymer and solvent additives strongly influence the discharge capacity and potential of LiFePO₄ electrodes at fast rates. The initial impedance and the direct current resistance were correlated with the discharge performance at high rate. The optimized amount of PEDOT:PSS added within the bulk resulted in lower value of impedance, lower load resistance and higher capacity as compared to the standard preparation. Furthermore ⁵⁷Fe Mössbauer spectroscopy and X-ray photoelectron spectroscopy were employed to probe the bulk transformation of the LiFePO₄ active material and the surface changes of the composite electrodes with conducting polymer upon lithiation. The electrode with PEDOT:PSS coated on the aluminium current collector and doped by ethylene glycol showed highly competitive performance (132 mAh/g at 5C and 145mAh/g at 2C for 50 cycles).

Introduction

Lithium ion batteries are the current choice for powering consumer electronics and are considered for use in electric vehicles and stationary back-up for renewable energy sources. The electric vehicles and power gadgets require batteries able to sustain high charge/discharge currents safely, provide high energy density and long cycle life. In present's Li-ion batteries, the positive electrode (cathode) imposes performance and costs requirements that limit the implementation of a sustainable market for electric cars.

The pioneering work of Padhi et al.¹ on lithium transition metal phosphates (LiMPO₄, M: Fe, Mn, Co, Ni) as positive-electrode materials set the cornerstone for the development and commercialization of lithium iron phosphate (LiFePO₄), a new generation material that offers safety and performance advantages over typical LiCoO₂. Besides, LiFePO₄ (LFP) is considered as environmentally friendly and can be produced at competitive cost by different synthetic routes.^{2,3} In spite of their outstanding features, the low intrinsic conductivity of lithium transition metal phosphates, ranging from 10⁻⁷ to 10⁻¹¹ S/cm for LFP,^{4,5} was considered as the limiting factor to achieve fast lithiation/delithiation in these materials.

However, it was later demonstrated that structural and compositional modifications of the surface and the bulk of

LiFePO₄ can turn it into a high rate material. For instance, the ionic diffusivity of LFP has been improved by lowering the diffusion paths along the less impeded [010] direction in nanoparticles⁶ or by coating the surface of LFP with glassy lithium pyrophosphate.⁷ For the enhancement of electronic conductivity of LFP, the currently adopted strategy consists in carbon-coating the active material particles through ball milling with inorganic carbon or by calcination of organic carbonaceous compounds.^{8,9} In order to ensure the electronic connection between particles and to the current collector, composite electrodes are formed using carbon additives in combination with polymeric binders like polyvinylidene fluoride (PVDF).

Conducting polymers are known for their excellent electronic properties and mechanical stability. These polymers can be utilized for the design of composite electrodes in order to increase conductivity without penalizing the electrochemical performance.^{10,11} In particular for LiFePO₄, composites with polyaniline,^{12,13} polypyrrole^{14,15} and polythiophene^{16,17} derivatives have been prepared by blending LFP with chemically synthesized polymers or by chemical or electrochemical polymerization in presence of the phosphate.¹⁸⁻²⁰ Recently, we reported on the improved performance of LFP-conducting polymer composites obtained directly over LFP-based electrodes by electrodeposition in acetonitrile medium²¹ and on the battery electrode by polymerization of alkylendioxythiophene-based monomers under battery operation conditions.²²

In our present approach to further improve the performance of LFP-based electrodes, mixed conductor poly(3,4-ethylenedioxythiophene)-poly(styrene sulfonate) (PEDOT:PSS) has been used as a conducting additive to develop an

^a Laboratorio de Química Inorgánica, Campus de Rabanales, Universidad de Córdoba, 14071, Spain.

^b Abengoa Research, Abengoa, C/ Energía Solar nº 1, Campus Palmas Altas, Seville, 41014, Spain

^c Email :shahzada.ahmad@abengoa.com, Ph:+34955404890

† Footnotes relating to the title and/or authors should appear here.

Electronic Supplementary Information (ESI) available: Fitted parameters for Mössbauer spectra and for XPS Fe(2p) and S(2p) spectra. See DOI: 10.1039/x0xx00000x

ionic/electronic conducting network for interconnection of the LFP particles. PEDOT:PSS is commercial product and provides conductivity due to the coexistence of the PEDOT electron conducting phase complexed with polystyrene sulfonate (PSS), where the sulfonate group is able to solvate Li^+ ions.²³ Besides, the conductivity of PEDOT:PSS can be further increased 2-3 orders of magnitude by the use of additives (so-called secondary doping) with oxygenated compounds like ethylene glycol or dimethyl sulfoxide.^{24,25}

In order to discern the main contribution from PEDOT:PSS to the conductivity of the LFP-based composite electrodes, we investigated the effects of the conducting polymer when it is coated over the aluminium current collector and/or dispersed within the bulk of the electrode.

Experimental Section

LiFePO_4 (LFP) was synthesized as described elsewhere.²⁶ Standard LFP electrodes (standard) were prepared by dispersing the active material with carbon black (CB) and polyvinylidene fluoride (PVDF) (85:8:7 by weight) in N-methyl pyrrolidone. The obtained ink was deposited over an aluminum current collector (0.64 cm^2) and dried at 80°C under vacuum for 12 h. The average load of LFP in the electrodes was estimated to be 5-6 mg/cm^2 .

Commercial PEDOT:PSS polymer aqueous dispersion 1.1 % w/w (Clevios PH1000, Heraeus) was filtered using Whatman $0.45 \mu\text{m}$ pore size filters. The conducting polymer was incorporated to the LFP-based electrode in three different ways: i) over the current collector, ii) in the bulk, and iii) both over the current collector and in the bulk. The PEDOT:PSS coating over the current collector was achieved by drop-casting the polymer dispersion ($30 \mu\text{L}/\text{cm}^2$) and allowing it to dry at 100°C for 24 h under vacuum. Afterwards, the LFP-based ink was deposited over PEDOT:PSS-coated aluminum and the electrode was finished as described above for the standard sample. The second preparation consisted in blending LFP with CB, PVDF and PEDOT:PSS (79:7:7:7 or 84:8:7:1 by weight) to form the electrode in a similar fashion as carried out for the standard LFP-based electrodes (see above). Finally, both methods were combined in order to form an electrode containing PEDOT:PSS both over the Al current collector and in the bulk. The different samples will be referred to as: *collector*, *bulk*, and *coll-bulk*, respectively, considering where the polymer is present in the electrode. Finally, all the electrodes were pressed at $1.5 \text{ ton}/\text{cm}^2$. To further enhance the PEDOT:PSS conductivity either 5 % v/v ethylene glycol (EG) or dimethyl sulfoxide (DMSO) was used as an additive for the polymer dispersion.

Test batteries were assembled in two or three-electrode Swagelok-type cells using the above mentioned LFP-based electrodes, Whatman glass-paper separator soaked with electrolyte (1M LiPF_6 in ethylene carbonate:diethyl carbonate, 1:1 weight ratio) and lithium metal foil as reference/counter electrode. All the cells were assembled inside a glove box under controlled argon atmosphere (H_2O , $\text{O}_2 < 1 \text{ ppm}$).

Galvanostatic cycling at different C-rates ($1 \text{ C} = 1 \text{ Li h}^{-1} \text{ mol}^{-1}$) was carried out at room temperature using a Biologic VMP or MPG station. The cut-off potential for charge and discharge were set at 4.2 and 2.2 V (vs. Li^+/Li), respectively. Electrochemical impedance spectra (EIS) were recorded in a Biologic SP-150 equipment using a three-electrode Swagelok-type cell with the LFP-based composite as working electrode, lithium counter electrode and lithium reference electrode. The applied sinus amplitude was fixed at 10 mV and the frequency was scanned from 1 MHz to 10 mHz.

X-ray photo electron spectroscopy (XPS) studies were performed with a Phoibos 150MCD (SPECS) instrument under vacuum (4.10^{-9} mbar) at room temperature with an $\text{Mg K}\alpha$ source. Prior to the analysis, all the samples were maintained overnight inside the chamber under constant vacuum. The samples taken from test batteries were rinsed by propylene carbonate solvent, dried and then carefully transferred into the instrument's chamber minimizing the contact with the external atmosphere. Fitting of the experimental spectra was performed with the CasaXPS software, applying Gaussian-Lorentzian symmetric or asymmetric line shapes and considering the software's library of relative sensitivity factors for the quantitative analysis. The energy scale was referenced to the C1s level (285 eV) from adventitious carbon.

^{57}Fe Mössbauer spectra were recorded at room temperature using an EG&G spectrometer at constant transmission and acceleration mode. The gamma radiation source was ^{57}Co (Rh matrix). The sextet lines recorded for high-purity iron foil were used to calibrate the velocity scale. The fitting of the spectra to Lorentzian profiles was carried out by a least square method using the WinISO software. The microstructure was imaged with the use of Hitachi S5200 field-emission scanning electron microscope (FE-SEM) operated at 5.0 keV

Results and Discussions

Figure 1 presents SEM images of the LFP-based standard electrode and different electrode preparations incorporating PEDOT:PSS. The standard electrode was composed of varying shaped LFP particles (ca. 80-300 nm), homogeneously mixed with CB and PVDF (Figure 1a). The cross-section view (Figure 1b) shows that the porosity was preserved though the sample was pressed to improve the contact to the current collector and between particles. Figure 1c shows a cross-sectional profile of the PEDOT:PSS deposit used for the *collector* sample. The PEDOT:PSS film (ca. $3 \mu\text{m}$) forms into a compact lamellar structure rich in PSS phase as previously described.²⁷ Figure 1d displays a close view of the composite formed by the *collector* method, where the PEDOT:PSS film over the current collector provides a compatible surface for the active material particles. The texture of the *bulk 1%* and *bulk 7%* electrodes can be observed in Figure 1e and Figure 1f. The primary particles in the bulk appear embedded in a continuous PEDOT:PSS network, the polymer acted as a glue that provides mechanical and conductive interconnection between LFP active particles. The texture and cross-section profiles for the *coll-bulk* samples were very similar to the features of the *bulk* electrodes.

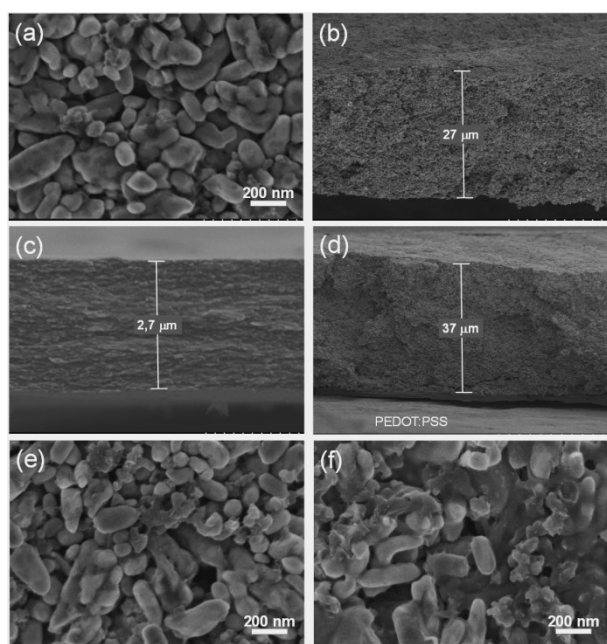


Figure 1. SEM images. a-b) Particles and cross-section of LFP standard electrode, c) PEDOT:PSS film formed over aluminium current collector, d) collector sample, e) bulk 1% sample and f) bulk 7% sample.

Mössbauer spectroscopy was used to investigate the oxidation state of iron in the pristine LFP-based electrode (Figure 2a). The Mössbauer spectrum of this sample features an intense doublet with characteristic hyperfine parameters typical of high spin Fe^{2+} ions in distorted octahedral coordination ($IS = 1.22 \text{ mm/s}$ and $QS = 2.96 \text{ mm/s}$) as previously reported.^{26,28,29} The fitting was improved by considering the contribution of an additional, less intense doublet ($IS = 0.48 \text{ mm/s}$ and $QS = 0.79$) ascribable to FeP, which was formed under the carbothermal, reducing synthesis conditions^{26,30} and constitutes $\sim 7\%$ of the total iron content in the pristine electrode.

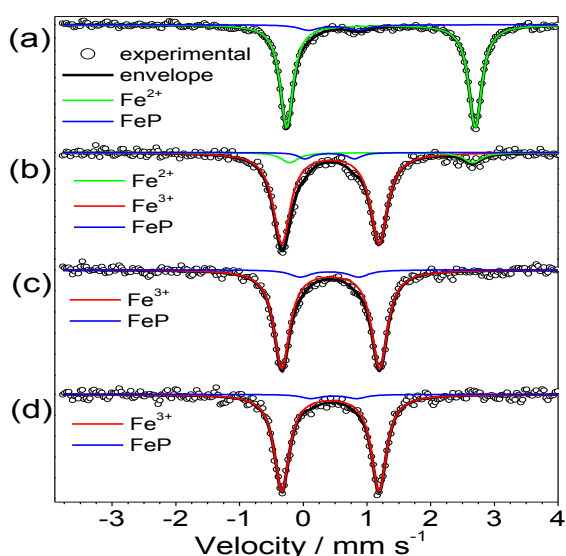


Figure 2. Mössbauer spectra of a) pristine LFP-based electrode, and charged electrodes: b) LFP-based, c) bulk 1% and d) EG-bulk 1%

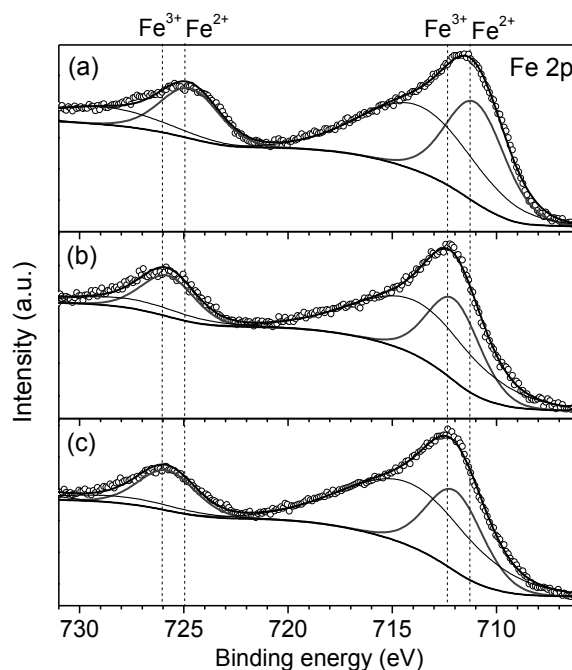


Figure 3. Fe(2p) XPS spectra of a) pristine LFP electrode and two charged electrodes with conducting polymer: b) bulk 1% and c) EG-bulk 1%.

In order to complement the sample analysis, XPS was used to characterize the pristine state of the surface of the standard electrode. Figure 3a presents the XPS signal of the Fe(2p) core levels. By comparing the peak position with the usual location of Fe^{3+} and Fe^{2+} marked with dashed lines in Figure 3, it can be concluded that in the pristine sample iron exists as Fe^{2+} with $2p_{3/2}$ and $2p_{1/2}$ splitted levels at binding energy values of ca. 711 and ca. 725 eV, respectively, in accordance with previous reports for LiFePO_4 .^{31,32} The broad signals at ca. 714 and ca. 728 eV correspond to satellite signals. The characteristic signals of FeP were un-resolved, which suggest a lower proportion of this impurity on the surface of the electrode.

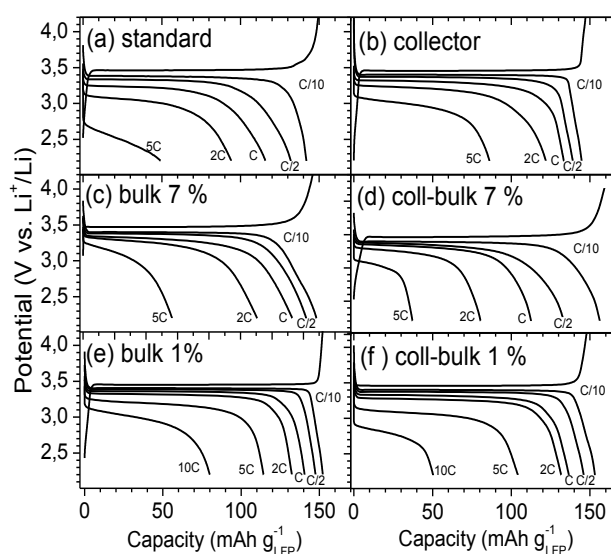


Figure 4. Initial discharge profiles at increasing rates for the different LFP-based composite electrodes.

Figure 4a presents the initial charge at C/10 and the discharge profiles at increasing rates for the LFP standard sample. The characteristic charge/discharge plateaus are centred near the equilibrium potential for the redox pair $\text{Fe}^{3+}/\text{Fe}^{2+}$ at 3.43 V, with a charge/discharge polarization of ca. 69 mV. The initial charge capacity of ca. 149 mAh/g corresponds to 0.88 mole of lithium extracted from LiFePO_4 . This value indicates a limited active material utilization as confirmed by Mössbauer spectroscopy of the charged sample (Figure 2b) that shows a considerable contribution of ca. 10 % of the total iron assigned to Fe^{2+} , according to the hyperfine parameters presented in Table S1.

The reduced charge efficiency is evident upon lithium reinsertion as the discharge capacity of 144 mAh/g corresponds to 85 % of the theoretical capacity for LiFePO_4 (Q_{theo} : 170 mAh/g). Although iron phosphide is known to improve the electronic conductivity of LiFePO_4 particles,^{29,33} its presence generates a detriment of the overall electrode's capacity. The performance of the LFP electrode at higher currents shows that the capacity decreases while the polarization increases due to transport limitations, as not all the particles can sustain high rates.³⁴ Thus, at 5C, the discharge capacity drastically decreases to 50 mAh/g and the discharge potential at half of the total delivered capacity ($E_{Q_{1/2}}$) reaches 2.49 V. This value translates into a poor energy and power density.

Aiming to improving the active material utilization, a PEDOT:PSS film was formed over aluminium to act as a conductive interface to promote the electrical contact of LFP particles to the current collector. The initial capacity (145 mAh/g) for this *collector* sample (Figure 4b) is the same as for the standard preparation. However at 5C, the higher capacity (86 mAh/g) and the higher discharge potential ($E_{Q_{1/2}}$: 2.97 V at 5C) indicates an improvement in the energy and power density. The effect of PEDOT:PSS present within the bulk of the electrode was also tested. Figure 4c shows that for the *bulk 7 %* sample, PEDOT:PSS shows beneficial impact on the discharge voltage ($E_{Q_{1/2}}$: 3.05 V at 5C) with no capacity improvement at low and fast rates ($Q_{C/10}$: 148 mAh/g, Q_{5C} : 56 mAh/g).

In order to take advantage of the features found for the *collector* (high capacity) and the *bulk* (high voltage) preparations, these architectures were simultaneously applied to form a single composite electrode with PEDOT:PSS coated over the aluminium current collector and also blended in the bulk (7 % w) of the electrode. The resulting preparation was named *coll-bulk 7%*. For the initial discharge, this preparation (Figure 4d) provided ca. 92 % of Q_{theo} . However, at 5C, the discharge capacity faded to 32 mAh/g, thus indicating an inefficient use of the active material. Despite the inferior rate capability of this *coll-bulk 7%* sample, its discharge potential ($E_{Q_{1/2}}$: 3.01 V) holds near the level found for the *collector* sample, although its power density is expected to drop as a consequence of the lower proportion of active material.

As a way to increase the gravimetric energy and power density of the LFP-based electrodes, the amount of PEDOT:PSS additive in the bulk was reduced to 1 % w. In this manner, the

bulk 1% preparation provided ca. 90 % of the theoretical capacity at C/10 in discharge, a value considerably higher than the observed for the standard LFP sample (83 %). The improved performance of the *bulk 1%* sample was confirmed at faster rates as the discharge capacity at 5C reaches 114 mAh/g (Figure 4e) and it was possible to discharge ca. 50 % of the theoretical capacity in 6 minutes (10C rate) at $E_{Q_{1/2}} \sim 2.96$ V. These observations reflect a higher efficiency for the lithium extraction/re-insertion linked to the Fe^{2+} to Fe^{3+} oxidation when a small amount of PEDOT:PSS is present in the bulk of the electrode. It was further supported by Mössbauer spectroscopy and XPS of the charged *bulk 1%* sample. The Mössbauer spectrum (Figure 2c) shows a symmetric doublet assigned to Fe^{3+} , while no Fe^{2+} doublet could be resolved. As expected, most of the iron in the charged electrode is ascribable to Fe^{3+} and the contribution from the FeP component is similar to that of the pristine LFP electrode (Table S1). Figure 3b presents the Fe(2p) XPS spectrum of the charged *bulk 1%* sample. The position of the Fe(2p_{3/2}) and Fe(2p_{1/2}) bands appear at ca. 1.1 eV, shifted to higher binding energy compared to the pristine LFP-based electrode (Table S2). This shift has been described previously and it is attributed to the Fe^{2+} to Fe^{3+} oxidation.^{31,32} The characteristic signals of FeP were not resolved neither at the Fe(2p) region nor at the P(2p) region (not shown).

Regarding the electrochemical performance of the *coll-bulk 1%* sample (Figure 4f), it also showed improvement in terms of capacity at 5C (104 mAh/g) with respect to its *coll-bulk 7%* analogue and to the standard electrode, although its performance at 10C is inferior to that achieved by the *bulk 1%* preparation. Therefore, 1 % wt. of conducting polymer in the bulk is pointed out as the optimum strategy to achieve high rate performance with undoped PEDOT:PSS.

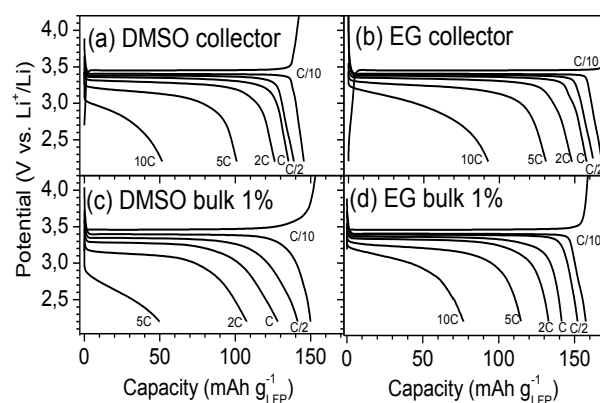


Figure 5. Initial discharge profiles at increasing rates for the different LFP-based composite electrodes with doped PEDOT:PSS.

Figure 5 shows the discharge profiles of the LFP-based composites with PEDOT:PSS treated with EG and DMSO conductivity enhancement agents, and tested for the *collector* and *bulk 1%* preparations. Both additives act as an agent to increase the conductivity of PEDOT:PSS by 2-3 orders of magnitude, reaching values as high as 1000 S/cm for 5% v/v

DMSO.³⁵ Thus, for the *collector* preparation with DMSO (Figure 3a), we found substantial improvement for both the capacity (101 mAh/g) and the discharge potential ($E_{Q1/2}$: 3.1 V) at 5C, as compared to its undoped analogue (Figure 4b).

Ethylene glycol boosted the performance of the *collector* preparation even further as it discharges higher capacity at 5C (132 mAh/g) and also at 10C (93 mAh/g) as shown in Figure 5b. For the *bulk 1%* preparations, doping with DMSO was ineffective as its discharge characteristics are very similar to those of the standard sample (see Figure 4a). Compared to the undoped *bulk 1%* preparation (Figure 4e), EG-doped sample showed similar capacity values at fast rates, with a substantial improvement on the discharge potential at 10C ($E_{Q1/2}$: 3.03 V). Similarly to the undoped *bulk 1%* sample, the Mössbauer spectroscopy and XPS of the EG-*bulk 1%* sample (Figure 2d and Figure 3c, respectively) showed no signals ascribable to Fe^{2+} , indicating that the oxidation of Fe^{2+} to Fe^{3+} was complete. As observed for the standard and the *bulk 1%* preparations, FeP was detected by Mössbauer spectroscopy of the charged EG-*bulk 1%* sample (Table S1). From the results presented above, it is evident that the incorporation of undoped and doped PEDOT:PSS has a beneficial impact on the discharge performance of the composite electrodes at high rates.

Several studies have explained the mechanism of the conductivity enhancement of PEDOT:PSS with secondary dopants in terms of the segregation of the insulating, excess PSS phase.^{36,37} Ethylene glycol (EG) and dimethylsulfoxide (DMSO) are among the most common secondary dopants. Also the modifications of the conformation, the size and morphology of PEDOT:PSS, have been pointed out as reasons for the conductivity improvement of PEDOT:PSS, as supported by atomic force microscopy and XPS.³⁷⁻³⁹ In particular, the segregation of the PSS phase has been correlated to the decrease of the PSS/PEDOT ratio, which can be estimated from the intensity ratio of the well resolved S(2p) XPS signals attributed to PSS and PEDOT sulphur atoms of different bonding environment.³⁹ We applied this approach to estimate the PSS/PEDOT ratios of undoped and EG-doped polymer deposits over the current collector and for the *bulk 1%* preparations in pristine and charged state.

Figure 6 presents the XPS plots of the S(2p) levels of the different samples. The S(2p) spectra of all the samples with PEDOT:PSS display two peaks, irrespective of the charge state or the presence of EG secondary dopant. The lower binding energy peak is attributed to the sulphur atoms in PEDOT. Due to the presence of electronegative oxygen atoms in the sulfonate fragments, the characteristic peak of PSS appears at higher binding energy. The two peaks were deconvoluted into doublets according to the $S(2p_{3/2})$ and $S(2p_{1/2})$ spin-orbit splitting. An asymmetric peak shape was considered for the PEDOT doublet in order to account for the positive charge delocalization over adjacent PEDOT rings.³⁷

The signals of neutral and ionic polystyrene (PS) sulfonate ($PS-SO_3H$ and $PS-SO_3^-$) are commonly separated by an energy of ca. 0.4 eV,³⁹ resulting in a high overlapping that leads to accuracy problems in the signal resolution. Taking this disadvantage under consideration, we used only one component for the refinement of these spectra. The results of the fitting and the quantitative analysis are listed in Table S3.

Figure 6a-c shows the samples with undoped PEDOT:PSS. A comparison of the XPS signals of the pristine and the charged PEDOT:PSS deposit over aluminum shows that the chemical environment of sulphur is preserved after the initial charge inside a test battery. The variation of the PSS/PEDOT ratio from 3.7 in the pristine state to 3.33 in the charged state, indicates a slight decrease of the PSS amount upon charging. This finding suggests a modification of the PEDOT:PSS complex in the presence of the battery electrolyte, where the acidic PSS fragment could react with $LiPF_6$ according to Eq. [1]. $LiPF_6$ is known for suffering decomposition reactions in presence of water and other acidic species.^{40,41} If a fraction of PSS were engaged in the reaction represented in Eq. [1], then PF_6^- could act as an alternative counterion for positively charged PEDOT. Conductivity values ranging from 100-300 S/cm have been reported for electropolymerized PEDOT films doped with PF_6^- .⁴²⁻⁴⁴ The microstructures (pores) in such thin films show different morphology depending on the size of the anion and the cation from the electrolyte used in the polymerization.⁴⁵

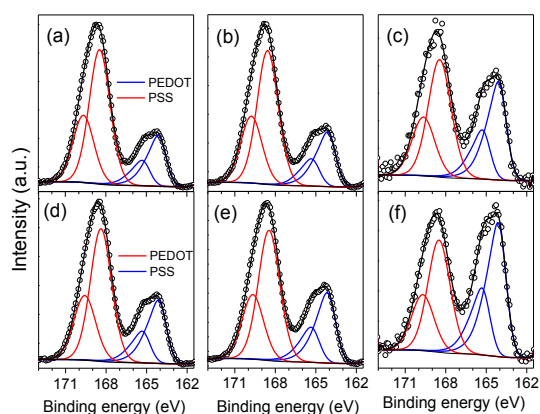


Figure 6. XPS plots of the S(2p) core level of undoped (a-c) and EG-doped samples (d-f). a) PEDOT:PSS, b) PEDOT:PSS @ C/10, c) bulk 1% @ C/10. d) EG-PEDOT:PSS, e) EG-PEDOT:PSS @ C/10, f) EG-bulk 1% @ C/10.

For the *bulk 1%* sample the PSS/PEDOT ratio of 1.74 indicates a more pronounced decrease of the PSS phase. This observation could arise from a combination of the PF_6^- counterion effect described above, and also to a certain extent from the contact with *N*-methyl pyrrolidone (NMP) that was used as solvent for the PVDF binder during the electrode preparation. In the past the conductivity enhancement of PEDOT:PSS by NMP treatment was reported and reasoned in terms of a decrease of the thickness of the excess, insulating PSS phase.^{36,46} The EG-doped samples showed the same tendency in the PSS/PEDOT ratio variation upon charging as observed for undoped samples. However, the use of EG as secondary dopant causes a more pronounced reduction of the PSS/PEDOT ratio, in agreement with previous observations.^{37,47} Thus, the charged EG-*bulk 1%* sample shows the lowest

PSS/PEDOT ratio of ~ 1.19 , indicating a notably large decrease of the PSS content.

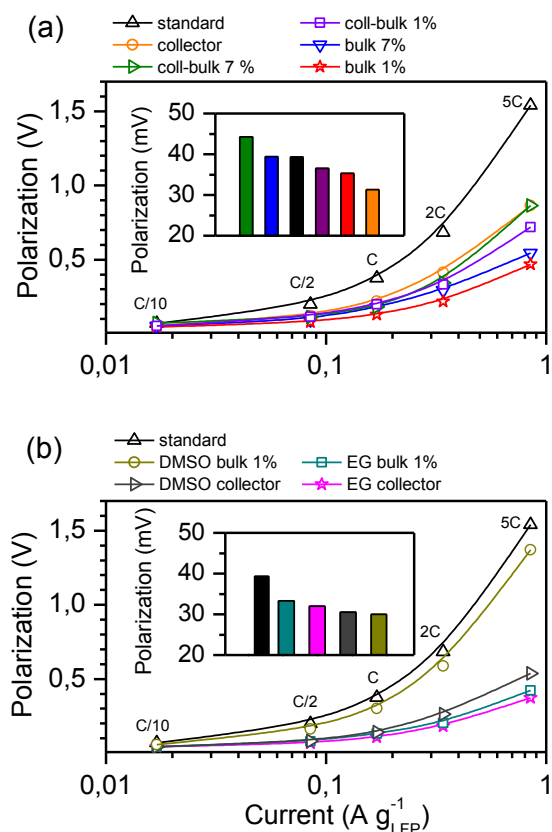


Figure 7. Charge/discharge polarization plots of the standard and the different LFP-based composite electrodes with a) undoped PEDOT:PSS and b) doped PEDOT:PSS with EG or DMSO. Inset: comparison of the zero-current polarization (computed by extrapolation).

Figure 7 presents the charge/discharge polarization of the different samples as a function of the charge/discharge current. Polarization tends to increase with the rate due to the thermodynamics of the de-lithiation/lithiation reaction in LFP, and also due to the transport hindrance through the electrode interfaces.⁴⁹ In the absence of PEDOT:PSS, the polarization can be as high as 1.54 V at 5C, resulting in a poor charge/discharge energy efficiency for the standard sample. Among the undoped samples (Fig. 7a), the *bulk 1%* architecture has the lowest polarization at 5C (0.54 V), which is almost three times lower than the value for the LFP standard sample. For the undoped samples the polarization tends to increase with the amount of PEDOT:PSS. Interestingly, at 5C the polarization of the *coll-bulk 7%* sample matches the value found for the *collector* sample. These observations suggest the existence of a threshold where the amount of undoped polymer in the bulk has no beneficial effect at high rate. Regarding the doped samples, the *collector* and *bulk 1%* preparations with EG showed the lowest polarization at 5C: 0.42 and 0.37 V respectively. We verified that DMSO had little effect on the polarization of the *bulk 1%* (0.54 V) and the *collector* (1.37 V) preparations.

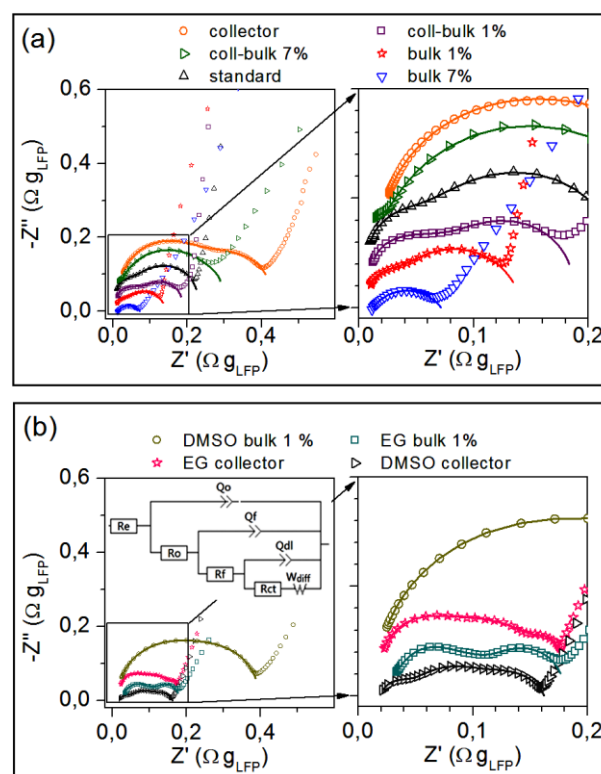


Figure 8. Impedance spectra of the standard and the different LFP-based composite electrodes with a) PEDOT:PSS and b) PEDOT:PSS doped with EG or DMSO. Inset: Equivalent circuit used to fit the experimental data (hollow circles).

Dreyer et al.⁴⁹ described the thermodynamical origin of the charge/discharge hysteresis (polarization) in $LiFePO_4$ at nearly zero current (20 mV @ C/1000), which arises from the inherent multiple-particle equilibria involving Li^+ insertion-extraction. It is expected that these equilibria were affected by the presence of PEDOT:PSS that acts as mixed ionic and electronic network with enhanced charge transport. We estimated the zero-current polarization for the different samples (insets in Figure 7) by extrapolation of linear plots Polarization vs. Current (not shown). The value determined for the standard LFP sample was 40 mV and differs to the reported value of 20 mV,⁴⁸ most probably due to different charge characteristics of our sample. To support our estimation, we recorded a charge/discharge cycle for standard $LiFePO_4$ at C/200. The experimental value was 48 mV, while at C/10 the polarization was 69 mV.

Among the undoped samples (inset Figure 7a) the *collector* preparation has the lowest zero current polarization value (31 mV), which contrasts with its high polarization values found at higher currents. For the samples containing PEDOT:PSS in the bulk, low amounts of PEDOT:PSS results in lower zero-current polarization, namely: 35 mV for *bulk 1%* compared to 40 mV for *bulk 7%*. Regarding the doped samples, the zero-current polarization values are very similar, ranging from 29 to 33 mV. Thus, we suggest that the presence of a conducting medium between the current collector and the active particles is crucial to promote their electronic connectivity and improve the current distribution and charge collection/delivery efficiency, especially at high rates.

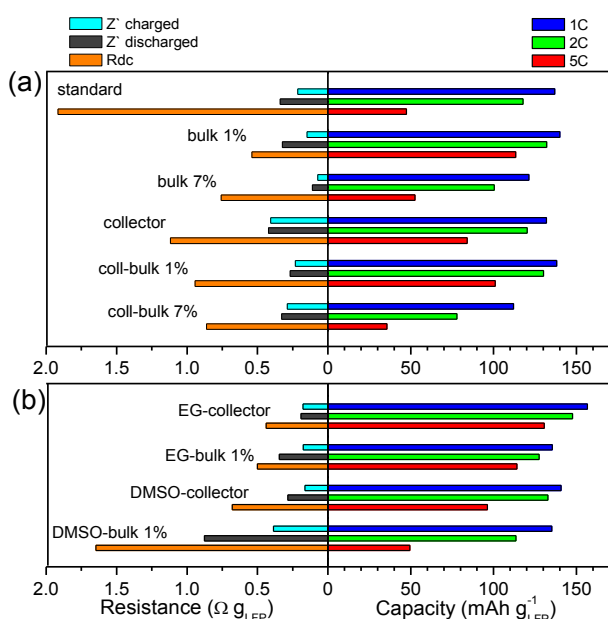


Figure 9. Discharge capacity and resistances for the standard and the different LFP-based composite electrodes with a) PEDOT:PSS and b) PEDOT:PSS doped with EG or DMSO. Z' and R_{dc} refer to the real part of the impedance and the direct current resistance, respectively.

Figure 8 presents the impedance spectra of the different samples after the initial charge at $C/10$. A previously reported equivalent circuit⁴⁹ was used to estimate the high-to-mid frequency resistance. In that equivalent circuit (showed in the inset of Figure 8), R_e corresponds to the electrolyte resistance, R_0 and Q_0 , respectively, to the resistance and capacitance of the interface between the current collector and active material particles (including additives). The sum in series of the charge transfer resistance (R_{ct}) and the diffusion impedance (Z_w) is added in parallel to the interfacial (double layer) capacitance (Q_{dl}) that develops around active particles. The resistance (R_f) and capacitance (Q_f) of films (eg. SEI) formed around the active particles are also considered in the model. In order to improve the quality of the fitting, constant phase elements (Q) were used instead of simple capacitors.

In the spectra (Figure 8a), three features considered in the equivalent circuit can be distinguished at different frequency ranges for undoped samples, namely: two depressed semicircles in the high and mid frequency range and the diffusional tail at lower frequencies. Additionally, for the samples with PEDOT:PSS over the current collector, a small bump is distinguishable at high frequencies. The spectra of EG and DMSO-doped samples (Figure 8b) has similar features as for undoped samples, however at high frequency the semi-arc is better resolved in the *collector* samples with EG and DMSO, which highlights the attribution of this feature to the interface between the conducting polymer-coated current collector and the active material particles.

In order to obtain comparative resistance values for the different samples we considered only the high to mid frequency range ($1 \text{ MHz} > \nu > 10 \text{ Hz}$). Figure 9 gathers the high-to-mid frequency impedance in charged and discharged states, correlated with capacity values at 1C, 2C and 5C. The

comparison of the impedance values in charged and discharged states shows how the electronic conductivity of all the samples is lower in the charged state. For LFP the lower impedance in charged state has been related to some rearrangement of particles when Li^+ ions are extracted from the phosphate.⁴⁹ For PEDOT and other conjugated polymers the lower impedance in charge is related to the higher conductivity in the p-doped oxidized state.⁵⁰ The initial impedance values in charged state reflect the quality of the electronic wiring throughout the electrode achieved during the preparation step. However, it is well known that new interfaces (e.g. SEI) develop as a function of time in open circuit and during the first charging/discharging of the battery. In order to gain further insight on the performance of the different samples, the direct current resistance (R_{dc}) at the voltage plateau was calculated from the slope of the Polarization vs. Current plot (not shown). Figure 9a shows that the higher the resistance of the standard LFP electrode, the lower the capacity at moderate and fast rates. This observation indicates that solely carbon black particles and PVDF are ineffective to ensure the connectivity of the active material particles, and highlights the importance of the electrode composition and architecture. The particle connectivity is notably improved by using a low amount of PEDOT:PSS mixed conductor in the *bulk 1%* electrode, resulting in a lower initial impedance and R_{dc} . The PEDOT:PSS network thus formed promotes the ionic and electronic wiring of the LFP particles, including their contact to the current collector. In this way the capacity increases as the charge is transferred and collected more efficiently throughout the electrode.

In the *bulk 7%* sample, the higher amount of polymer does improve the electronic conductivity of the electrode, as evidenced from its low initial impedance values. However, its lower capacity, compared to *bulk 1%*, could arise from an increase in the length of the conduction pathways at the PSS phase within the bulk.^{27,36,51} This condition limits the initial discharge performance and could affect the stability of the electrode for extended cycling.

The PEDOT:PSS coating on the aluminium current collector tends to increase its impedance because of the thickening of the conduction length and due to formation of aluminium oxide by reaction with the polystyrenesulfonic acid.⁵² Nevertheless, these drawbacks are compensated by an increase of the effective contact points between the aluminium current collector and the active material as the PEDOT:PSS coating acts as a plastic cushion that can adapt to the shape of LFP particles and accommodate them closely. This architecture results in a higher utilization of LFP and thus a higher capacity than the standard sample. The *coll-bulk 1%* combines the features of the *bulk 1%* and *collector* preparations, although this combination does not result in a synergistic effect. During the preparation of the *coll-bulk 7%* and *coll-bulk 1%* we noticed that the PEDOT:PSS dispersion present in the cathode slurry tends to dissolve the PEDOT:PSS film deposited on the collector. This was reflected in the higher polarization of these samples in Figure 7a and the higher direct current resistance shown in Figure 9a. For this reason we

discarded the *coll-bulk* preparations with EG or DMSO dopants.

Thus improvement in the conduction paths between the LFP particles by the presence of a three-dimensional (3D), conducting polymer network in the bulk leads to a higher discharge potential (lower charge/discharge polarization), which results in a higher power density of the battery. While, the better contact between the current collector and the electrode materials through a conducting PEDOT:PSS interface improves the active material utilization. This last characteristic was found for the EG-doped *collector* sample (Figure 9b), which yielded the highest capacity values among all the studied samples.

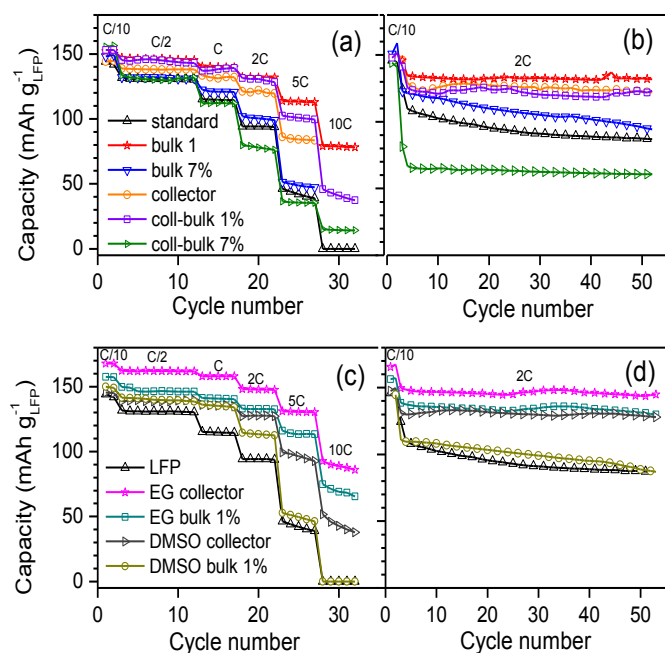


Figure 10. Cycling performance for the standard and the different LFP-based composite electrodes with PEDOT:PSS. a-b) Samples with PEDOT:PSS and c-d) samples doped with EG and DMSO.

Figure 10 presents the rate performance of the different samples as a function of the number of cycles. For undoped samples, the best performance at all rates is confirmed for the sample with the lowest amount of polymer, namely *bulk 1%*. This sample is able to discharge almost 50% of the theoretical capacity at 10C and delivers a stable capacity of 133 mA h/g_{LFP} at 2C for 50 cycles, which outperforms the *standard* sample. Further improvement of the discharge properties of LFP was achieved by coating the aluminium current collector with PEDOT:PSS doped with a small amount of ethylene glycol. This simple *EG collector* preparation has the best rate performance among all the tested electrode architectures as it can discharge 90 mAh/g_{LFP} at a fast rate of 10C, and deliver 145 mAh/g_{LFP} continuously at 2C during 50 cycles.

As previously reported by other authors, EG or DMSO increase the surface proportion of electron-conducting PEDOT in the final polymer film. Therefore EG-collector and DMSO-collector could present a more conducting PEDOT:PSS/Al interface at

which the charge collection could be efficient during cycling at high rates. For the undoped collector the surface proportion of non-conducting PSS is higher, therefore the less conducting PEDOT:PSS/Al interface could limit the charge collection at high rates.

Conclusions

LiFePO₄ electrodes were built in different architectures encompassing PEDOT:PSS conducting polymer. The incorporation of PEDOT:PSS additives within the bulk of the electrode was achieved by a simple blending technique and provides a three-dimensional, mixed conducting network that notably improves the performance of LiFePO₄. By using this method with the addition of a small amount of PEDOT:PSS resulted in high capacity values specially at high rates, achieving a reversible capacity of 114 mAh/g at 5C and 132 mAh/g at 2C for extended cycling. We found that the use of ethylene glycol as conductivity enhancement agent for PEDOT:PSS deposited over the aluminium collector is an effective strategy to boost the performance of LiFePO₄. The electrodes thus formed show lower load resistance with a discharge plateau above 3.0 V at high rates and deliver 132 mAh/g at 5C. These features and the excellent capacity retention of 145 mAh/g at 2C for the measured 50 cycles are attributed to the enhanced conductivity of EG-doped PSS that arises from the segregation of insulating PSS, as evidenced from the XPS analysis. The presented methods are easy to scale-up and could be applied to other electrode active materials for alkali ion batteries.

Notes and references

- 1 A. K. Padhi, K. S. Nanjundaswamy and J. B. Goodenough, *J. Electrochem. Soc.*, 1997, **144**(4), 1188.
- 2 C. M. Julien, A. Mauger, K. Zaghib, *J. Mater. Chem.*, 2011, **21**(27), 9950.
- 3 Y. Zhang, Q. Huo, P. Du, L. Wang, A. Zhang, Y. Song, Y. Lv, G. Li, *Synth. Met.*, 2012, **162**(13-14), 1315.
- 4 C. Delacourt, L. Laffont, R. Bouchet, C. Wurm, J.-B. Leriche, M. Morcrette, J.-M. Tarascon, C. Masquelier, *J. Electrochem. Soc.*, 2005, **152**(5), A913.
- 5 C. Zhu, K. Weichert, J. Maier, *Adv. Funct. Mater.*, 2011, **21**(10), 1917.
- 6 H. Huang, S.-C. Yin, L. F. Nazar, *Electrochem. Solid-State Lett.* 2001, **4**(10), A170.
- 7 B. Kang, G. Ceder, *Nature*, 2009, **458**(7235), 190.
- 8 N. Ravet, Y. Chouinard, J. F. Magnan, S. Besner, M. Gauthier, M. Armand, *J. Power Sources*, 2001, **97-98**, 503.
- 9 J. Wang, X. Sun, *Energy Environ. Sci.*, 2012, **5**(1), 5163.
- 10 A. D. Pasquier, F. Orsini, A. S. Gozdz, J.-M. Tarascon, *J. Power Sources*, 1999, **81-82**, 607.
- 11 A. V. Murugan, C. W. Kwon, G. Campet, B. Kale, T. Maddanimath, K. Vijayamohan, *J. Power Sources*, 2002, **105**(1), 1.
- 12 W. M. Chen, Y. H. Huang, L. X. Yuan, *J. Electroanal. Chem.* 2011, **660**(1), 108.
- 13 W. M. Chen, L. Qie, L. X. Yuan, S. A. Xia, X. L. Hu, W. X. Zhang, Y. H. Huang, *Electrochim. Acta.*, 2011, **56**(6), 2689.
- 14 I. Boyano, J. A. Blazquez, I. de Meatza, M. Bengochea, O. Miguel, H. Grande, Y. Huang, J. B. Goodenough, *J. Power Sources*, 2010, **195**(16), 5351.

- 15 G. X. Wang, L. Yang, Y. Chen, J. Z. Wang, S. Bewlay, H. K. Liu, *Electrochim. Acta*, 2005, **50**, 4649.
- 16 J. Liu, G. Yang, X. Zhang, J. Wang, R. Wang, *J. Power Sources*, 2012, **197**, 253.
- 17 Y. M. Bai, P. Qiu, Z. L. Wen, S. C. Han, *J. Alloys Compd.*, 2010, **508**(1), 1.
- 18 D. Lepage, C. Michot, G. Liang, M. Gauthier, S. B. Schougaard, *Angew. Chemie - Int. Ed.*, 2011, **50**(30), 6884.
- 19 H. C. Dinh, S. il Mho, I. H. Yeo, *Electroanalysis*, 2011, **23**(9), 2079.
- 20 N. D. Trinh, M. Saulnier, D. Lepage, S. B. Schougaard, *J. Power Sources*, 2013, **221**, 284.
- 21 *RSC Adv.*, 2014, **4**(50), 26108.
- 22 D. Cíntora-Juárez, C. Pérez-Vicente, S. Ahmad, J. L. Tirado, *Phys. Chem. Chem. Phys.*, 2014, **16**(38), 20724.
- 23 S. Guhathakurta, K. Min, *Polymer (Guildf)*, 2010, **51**(1), 211.
- 24 J. Ouyang, Q. Xu, C. W. Chu, Y. Yang, G. Li, J. Shinar, *Polymer (Guildf)*, 2004, **45**(25), 8443.
- 25 J. Y. Kim, J. H. Jung, D. E. Lee, J. Joo, *Synth. Met.*, 2002, **126** (2-3), 311.
- 26 B. León, C. Pérez-Vicente, J. L. Tirado, P. Biensan, C. Tessier, *J. Electrochem. Soc.*, 2008, **155**(3), A211.
- 27 A. M. Nardes, M. Kemerink, R. a J. Janssen, J. a M. Bastiaansen, N. M. M. Kiggen, B. M. W. Langeveld, A. J. J. M. Van Breemen and M. M. De Kok, *Adv. Mater.*, 2007, **19**, 1196.
- 28 B. Hannyer, A. a M. Prince, M. Jean, R. S. Liu and G. X. Wang, *Hyperfine Interact.*, 2006, **167**, 767.
- 29 Y.-H. Rho, L. F. Nazar, L. Perry and D. Ryan, *J. Electrochem. Soc.*, 2007, **154**, A283.
- 30 A. Andersson, B. Kalska, L. Haggstrom, J. O. Thomas, *Solid State Ionics.*, 2000, **130**(1-2), 41.
- 31 R. Dedryvère, M. Maccario, L. Croguennec, F. Le Cras, C. Delmas and D. Gonbeau, *Chem. Mater.*, 2008, **20**, 7164.
- 32 L. Castro, R. Dedryvère, M. El Khalifi, P. E. Lippens, J. Bréger, C. Tessier and D. Gonbeau, *J. Phys. Chem. C*, 2010, **114**, 17995.
- 33 C. W. Kim, J. S. Park, K. S. Lee, *J. Power Sources*, 2006, **163**(1 SPEC. ISS.), 144.
- 34 R. Malik, A. Abdellahi and G. Ceder, *J. Electrochem. Soc.*, 2013, **160**, A3179.
- 35 A. Elschner, S. Kirchmeyer, W. Lövenich, U. Merker and K. Reuter, PEDOT: Principles and Applications of an Intrinsically Conductive Polymer. CRC Press: Florida, 2010. Chapter 9, p. 122.
- 36 S. K. M. Jönsson, J. Birgersson, X. Crispin, G. Greczynski, W. Osikowicz, a. W. Denier van der Gon, W. R. Salaneck and M. Fahlman, *Synth. Met.*, 2003, **139**, 1.
- 37 X. Crispin, S. Marciniak, W. Osikowicz, G. Zotti, a. W. Denier Van Der Gon, F. Louwet, M. Fahlman, L. Groenendaal, F. De Schryver and W. R. Salaneck, *J. Polym. Sci. Part B Polym. Phys.*, 2003, **41**, 2561.
- 38 X. Crispin, F. L. E. Jakobsson, a Crispin, P. C. M. Grim, P. Andersson, a Volodin, C. van Haesendonck, M. Van der Auweraer, W. R. Salaneck and M. Berggren, *Chem. Mater.*, 2006, **18**, 4354.
- 39 G. Greczynski, T. Kugler and W. R. Salaneck, *Thin Solid Films*, 1999, **354**, 129.
- 40 U. Heider, R. Oesten and M. Jungnitz, *J. Power Sources*, 1999, **81-82**, 119.
- 41 T. Kawamura, S. Okada and J. I. Yamaki, *J. Power Sources*, 2006, **156**, 547.
- 42 A. Aleshin, R. Kiebooms, R. Menon, F. Wudl and A. Heeger, *Phys. Rev. B*, 1997, **56**, 3659.
- 43 A. Aleshin, R. Kiebooms, R. Menon and A. J. Heeger, *Synth. Met.*, 1997, **90**, 61.
- 44 I. Giurgiu, K. Zong, J. R. Reynolds, W. P. Lee, K. R. Brennehan, A. V. Saprigin, a. J. Epstein, J. Hwang and D. B. Tanner, *Synth. Met.*, 2001, **119**, 405.
- 45 A. I. Melato, M. H. Mendonça and L. M. Abrantes, *J. Solid State Electrochem.*, 2009, **13**, 417.
- 46 C.-H. Chen, L. Zhou and J. Lv, *J. Appl. Polym. Sci.*, 2012, **125**, 3134.
- 47 J. Ouyang, Q. Xu, C. W. Chu, Y. Yang, G. Li and J. Shinar, *Polymer (Guildf)*, 2004, **45**, 8443.
- 48 W. Dreyer, J. Jamnik, C. Gohlke, R. Huth, J. Moskon and M. Gaberscek, *Nat. Mater.*, 2010, **9**, 448.
- 49 J.-M. Atebamba, J. Moskon, S. Pejovnik and M. Gaberscek, *J. Electrochem. Soc.*, 2010, **157**, A1218.
- 50 J. Heinze, B. A. Frontana-Urbe and S. Ludwigs, *Chem. Rev.*, 2010, **110**, 4724.
- 51 T. Stöcker, A. Köhler and R. Moos, *J. Polym. Sci. Part B Polym. Phys.*, 2012, **50**, 976.
- 52 W. Bantikassegn and O. Inganäs, *Thin Solid Films*, 1997, **293**, 138.